JGR Atmospheres

RESEARCH ARTICLE
10.1029/2019JD031554

Key Points:
- High-resolution modeling captures key physical characteristics of extreme atmospheric rivers
- Fine scale is needed to well reproduce precipitation extremes and associated meteorological features
- Targeted simulations can advance the studying of atmospheric rivers changes to a warming climate

Supporting Information:
- Supporting Information S1

Correspondence to:
X. Huang,
xingyhuang@gmail.com

Citation:
Huang, X., Swain, D. L., Walton, D. B., Stevenson, S., & Hall, A. D. (2020). Simulating and evaluating atmospheric river-induced precipitation extremes along the U.S. Pacific Coast: Case studies from 1980–2017. *Journal of Geophysical Research: Atmospheres*, *125*, e2019JD031554. https://doi.org/10.1029/2019JD031554

Received 26 AUG 2019
Accepted 25 JAN 2020
Accepted article online 29 JAN 2020

Author Contributions
Conceptualization: Xingying Huang, Daniel L. Swain, Daniel B. Walton, Alex D. Hall
Funding Acquisition: Alex D. Hall
Methodology: Xingying Huang, Daniel L. Swain, Daniel B. Walton, Alex D. Hall
Formal Analysis: Xingying Huang
Investigation: Xingying Huang
Project Administration: Alex D. Hall
Supervision: Alex D. Hall
Visualization: Xingying Huang, Daniel L. Swain, Daniel B. Walton
Writing - review & editing: Xingying Huang, Daniel L. Swain, Samantha Stevenson, Alex D. Hall

Simulating and Evaluating Atmospheric River-Induced Precipitation Extremes Along the U.S. Pacific Coast: Case Studies From 1980–2017

Xingying Huang[1], Daniel L. Swain[2,3,4], Daniel B. Walton[1], Samantha Stevenson[5], and Alex D. Hall[1]

[1]Department of Atmospheric and Oceanic Sciences, University of California, Los Angeles, CA, USA, [2]Institute of the Environment and Sustainability, University of California, Los Angeles, CA, USA, [3]Capacity Center for Climate and Weather Extremes, National Center for Atmospheric Research, Boulder, CO, USA, [4]The Nature Conservancy of California, San Francisco, CA, USA, [5]Bren School of Environmental Science and Management, University of California, Santa Barbara, CA, USA

Abstract Atmospheric rivers (ARs) are responsible for a majority of extreme precipitation and flood events along the U.S. West Coast. To better understand the present-day characteristics of AR-related precipitation extremes, a selection of nine most intense historical AR events during 1980–2017 is simulated using a dynamical downscaling modeling framework based on the Weather Research and Forecasting Model. We find that the chosen framework and Weather Research and Forecasting Model configuration reproduces both large-scale atmospheric features—including parent synoptic-scale cyclones—as well as the filamentary corridors of integrated vapor transport associated with the ARs themselves. The accuracy of simulated extreme precipitation maxima, relative to in situ and interpolated gridded observations, improves notably with increasing model resolution, with improvements as large as 40–60% for fine scale (3 km) relative to coarse-scale (27 km) simulations. A separate set of simulations using smoothed topography suggests that much of these gains stem from the improved representation of complex terrain. Additionally, using the 12 December 1995 storm in Northern California as an example, we demonstrate that only the highest-resolution simulations resolve important fine-scale features—such as localized orographically forced vertical motion and powerful near hurricane-force boundary layer winds. Given the demonstrated ability of a targeted dynamical downscaling framework to capture both local extreme precipitation and key fine-scale characteristics of the most intense ARs in the historical record, we argue that such a configuration may be highly conducive to understanding AR-related extremes and associated changes in a warming climate.

1. Introduction and Background

A majority of annual precipitation along the U.S. West Coast originates from a few intense atmospheric river (AR) events each year, contributing up to half of the annual precipitation in some regions (Dettinger et al., 2011; Gershunov et al., 2017). These events, which are characterized by narrow and filamentary corridors of enhanced water vapor flux (Ralph et al., 2004; Zhu & Newell, 1998), are typically associated with extratropical cyclones over ocean basins and are responsible for the vast majority of poleward moisture transport in the midlatitudes (Nash et al., 2018). The synoptic characteristics and impacts of landfalling ARs over the Western United States have been well documented over the past decade (Dettinger et al., 2011; Guan & Waliser, 2015; Jackson et al., 2016; Kim et al., 2018; Rutz et al., 2014). These previous studies have found that the seasonal occurrence or lack of ARs can dictate flood or drought conditions in certain midlatitude regions, including California and most of the Pacific Coast of North America.

AR-driven precipitation extremes can be both beneficial in terms of water supply and hazardous in the form of flood risk, depending on their location, strength, and timing (Eldardiry et al., 2019; Pavelsky et al., 2011; Ralph et al., 2019). Evidence suggests that a majority of North American Pacific Coast floods and associated damages are caused by ARs (Konrad & Dettinger, 2017)—which can sometimes yield extraordinarily intense orographic precipitation rivaling that of landfalling tropical cyclones (Leung & Qian, 2009; Neiman et al., 2011; Ralph et al., 2006). One recent example of a highly consequential extreme AR with intense rainfall occurred in the Feather River watershed of Northern California (NC) during a series of AR events in February 2017, which escalated an engineering failure on the Oroville Dam to a crisis of national significance (Huang et al., 2018).

Using coarse-resolution global climate models (GCMs), several previous studies have concluded that most West Coast regions will experience an increase in AR intensity as the climate warms (Dominguez et al., 2012; Gao et al., 2015; Shields & Kiehl, 2016; Swain et al., 2018; Warner et al., 2015), although this increase may be counterbalanced by a decrease in frequency in some places (Espinoza et al., 2018)—suggesting that a more nuanced view regarding radiatively forced changes in AR properties is required. However, these results indicate that improving the collective understanding of intense ARs and associated precipitation extremes is of particular importance (Polade et al., 2014, 2017). GCM studies at coarse resolution, typically >100 km, can provide useful information on the large-scale environments associated with ARs—particularly the synoptic-scale cyclones that often drive the most extreme events. However, despite their relative strengths in a large-scale context, coarse-scale GCMs are typically not well suited to capturing realistic precipitation patterns and other fine-scale features that are most relevant for local impacts during extreme AR events, such as narrow corridors of extreme water vapor transport and orographically forced vertical motion (e.g., Dettinger et al., 2011).

High-resolution dynamical simulations of ARs are typically necessary to correctly capture the fine-scale features associated with AR-driven precipitation (Swain et al., 2015). This is especially true given the critical importance of orographic forcing by relatively steep but narrow topographical barriers, which is known to be a key mechanism of AR-generated precipitation extremes along the Pacific Coast region (Dettinger et al., 2011). Past studies have demonstrated that regional atmospheric model simulations, even at horizontal resolutions as coarse as dozens of km, can improve the representation of precipitation resulting from ARs as well as its spatial distribution in topographically complex regions (Huang & Ullrich, 2017; Leung & Qian, 2009). Dynamical downscaling of coarser initial data using limited-area regional weather models allows for greatly improved representation of mesoscale processes critical to precipitation formation, including resolved convection via nonhydrostatic dynamical cores (Leung et al., 2003; Mass et al., 2002), a more realistic approximation of small-scale processes and interactions with more sophisticated microphysics parameterizations, and improved depiction of orographically forced moist processes (Rummukainen, 2010).

We aim to investigate the ability of a dynamical downscaling framework to capture the spatial and temporal patterns of extreme precipitation that result from a set of particularly intense historical AR storms. Additionally, we explore the differing effects of model horizontal resolution from an atmospheric process perspective and improved resolution of complex topography with more realistic orography. We emphasize that the present study does not focus on developing a novel AR detection algorithm nor do we systematically test the sensitivity of simulated precipitation to a wide range of Weather Research and Forecasting Model (WRF) parameterizations. Instead, we focus on validating simulations of the most extreme ARs in the historical record for two key reasons. First, it is widely recognized that the most extreme precipitation events are responsible for a disproportionate fraction of societal impacts (e.g., IPCC 2012, Chapters 3 and 4; Field et al., 2012). Second, we hypothesize that higher spatial resolution simulations may be especially valuable in capturing fine-scale extreme values of relevant thermodynamic and kinematic variables, including precipitation, water vapor transport, and vertical motion. Our primary goals are therefore to (a) investigate the effects of resolution and topography on extreme precipitation, explicitly represented water vapor transport and vertical motion, as well as parameterized processes including precipitation, and (b) validate a modeling framework that could eventually be used to explore changes in extreme AR characteristics in warming climate, using a targeted focus on individual storm-scale extreme events.

In the present work, we go beyond previous studies to demonstrate the enhanced value of high-resolution downscaling as it pertains specifically to AR-related precipitation extremes. To do so, we use a highly targeted, individual storm-based case study approach that leverages a multiscale modeling framework. Unlike previous studies, which generally investigated ARs using multiyear simulations at the similar or coarser spatial resolution, our efforts specifically target the most extreme historical AR events across the U.S. West Coast between 1980 and 2017 most of which were storms that had notable societal impacts.

2. Methods and Modeling

2.1. AR Detection

We select nine of the most extreme historical AR events along the U.S. West Coast to be studied using our modeling framework. These events are chosen based on integrated water vapor transport (IVT) from relatively high-resolution reanalysis data sets (Ralph et al., 2019). To do so, we use 3-hourly MERRA-2 (Modern-Era Retrospective analysis for Research and Applications) reanalysis data (Rienecker et al., 2011) (~0.5°) to calculate IVT across the North Pacific Basin between 1,000 and 200 hPa at all time steps between January 1980 and December 2017. The appropriateness of using MERRA-2 for historical AR event selection is evidenced by its role as the reference data set in the Atmospheric River Intercomparison Project for AR detection (Shields et al., 2018).

We acknowledge that there are many options for AR detection and tracking with the most numerous AR catalogs distributed over the U.S. Pacific Coast. In this study, we do not develop an entirely new AR detection algorithm as our focus is on simulating a handful of especially extreme AR events across the U.S. West Coast. Instead, the method we use here borrows heavily from existing high-quality detection algorithms that have previously been validated as part of the aforementioned Atmospheric River Intercomparison Project for AR detection project (Shields et al., 2018). Our AR detection procedures first calculate the historical climatology during 1980–2017 at each MERRA-2 grid cell between 100–180° W and 10–70° N, which spans the northeastern Pacific Ocean basin. For each time step, the AR detection algorithm looks for connected sets of grid cells (i.e., objects) where IVT exceeds 250 kg/m/s above the daily climatology. Such objects that exceed 2,000 km in length and include at least one land grid cell along the U.S. West Coast are classified as landfalling ARs. If there are shared grid cells between a landfalling AR at time step n and another landfalling AR at time step $n + 1$, then those two ARs are tracked as part of the same event. Thus, an AR event is a collection of sequential steps during which landfall is occurring. As a result, our approach is regionally targeted and informed by specific regional background IVT conditions across the North Pacific basin (Chen et al., 2018; Ralph et al., 2010, 2013; Rutz et al., 2014). We point out that this metric is likely not appropriate for use outside of oceanic midlatitude regions, such as polar or tropical regions where background IVT is much lower or higher, respectively.

Further details about the AR detection procedures can be found in the supporting information. In general, two of the most intense ARs were selected from each region (Figure 1 and Table 1). The exception is for NC, which, due to its substantial latitudinal extent (see Figure 1), warranted the inclusion of a third AR. ARs were cross-referenced with historical accounts of storms to verify they existed and were of high magnitude. In total, nine ARs were selected, including two that made landfall over Southern California (SC, latitudinal band of 31.6–34.5° N), three over NC (34.5–42° N), two over Oregon (OR, 42–46.25° N), and two over Washington (WA, 46.25–49° N) (see Table 1 for event details). Distributions of AR intensity for all the historical ARs examined in this study at each landfalling region are shown in Figure 1.

2.2. Downscaling Experimental Design and Model Configuration

The WRF V3.8.1 (Skamarock & Klemp, 2008) is used in the present analysis. WRF has been used extensively in previous studies of general precipitation extremes, as well as specifically within an AR context (Eldardiry et al., 2019; Hughes et al., 2014; Leung & Qian, 2009; Martin et al., 2018; Pontoppidan et al., 1271). We use atmospheric reanalysis data (ERA-Interim) data (~80 km) to provide 6-hourly initial and boundary conditions to force the nested WRF simulations, including sea surface temperature. ERA-Interim has been widely used and validated for its reliability as forcing data in model simulations (Dee et al., 2011). Compared to the in situ aircraft observations of ARs over the northeastern Pacific, ERA-Interim IVT tends to accurately capture the key large-scale and mesoscale features of these events (Ralph et al., 2012). Additionally, we find that the selected AR events retrieved from the MERRA-2 for our study are very similar to the same events in the ERA-Interim data set using the AR detection method described in the previous subsection (see Video S1 in the supporting information). To accommodate the transition from relatively coarse ERA-Interim boundary conditions and the very high resolution simulations at 3 km over the U.S. West Coast, we use three nested domains of 27, 9, and 3 km (see Figure S1 for the detailed domain configuration). The outer two domains of 27 and 9 km cover a large part of the northeastern Pacific Ocean and the entire western U nited States.

The model physics parameterizations applied in this study include the New Thompson microphysics scheme (Thompson et al., 2008) Dudhia shortwave radiation scheme (Dudhia, 1989), Rapid Radiative Transfer

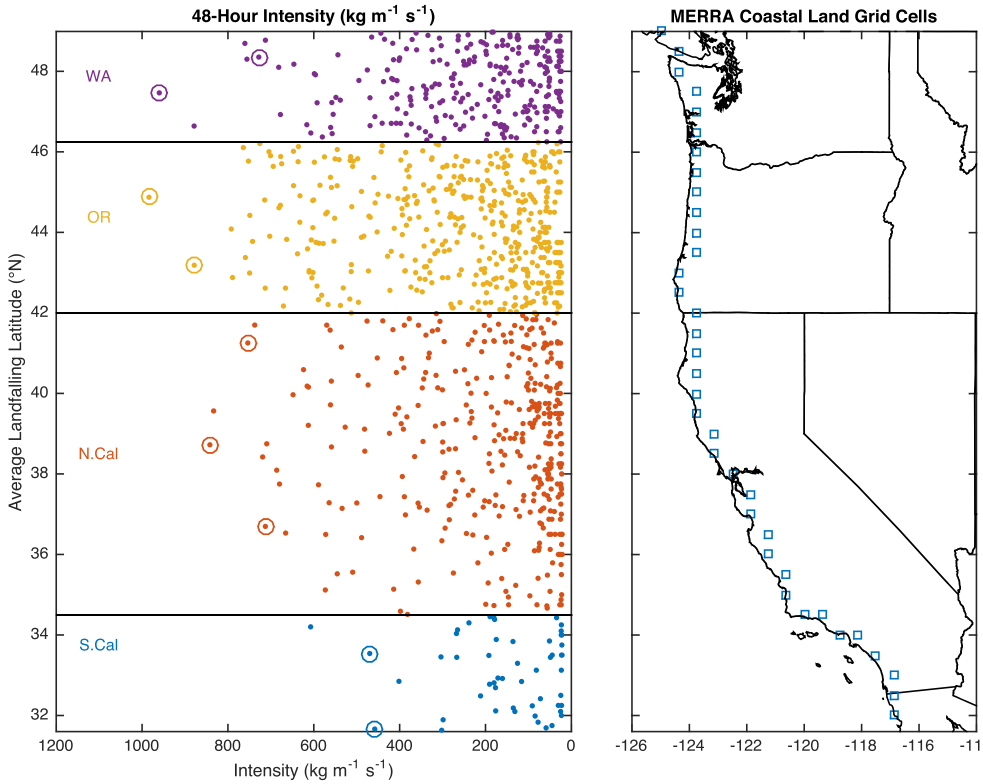

Figure 1. IVT Intensity of selected AR events in MERRA-2 reanalysis at different geographic points of landfall. Left: maximum 48-hr averaged IVT intensity versus landfalling latitude for ARs along the U.S. West Coast during the period years 1980–2017. ARs are binned by region: Southern California (31.6–34.5° N), Northern California (34.5–42° N), Oregon (42–46.25° N), and Washington (46.25–49° N). Circled dots refer to events simulated in this study. Right: coastal land grid cells used for AR selection from the MERRA-2 data set.

Table 1
Summary of the Nine Simulated ARs

Event ID	Average land falling latitude	AR dates	Dates downscaled	Average 48-hr intensity (kg/(m/s))
SC1	33.54	08-Jan-2005 to 10-Jan-2005	05-Jan-2005 to 12-Jan-2005	470
SC2	31.66	06-Jan-1993 to 08-Jan-1993	04-Jan-1993 to 11-Jan-1993	458
NC1	38.72	28-Dec-1996 to 03-Jan-1997	25-Dec-1996 to 03-Jan-1997	842
NC2	41.25	10-Dec-1995 to 13-Dec-1995	05-Dec-1995 to 16-Dec-1995	754
NC3	36.70	07-Jan-2017 to 09-Jan-2017	05-Jan-2017 to 10-Jan-2017	713
OR1	44.87	04-Nov-2006 to 08-Nov-2006	02-Nov-2006 to 11-Nov-2006	984
OR2	43.18	02-Dec-2007 to 04-Dec-2007	01-Dec-2007 to 07-Dec-2007	878
WA1	47.46	16-Oct-2003 to 19-Oct-2003	14-Oct-2003 to 23-Oct-2003	960
WA2	48.35	09-Nov-1990 to 11-Nov-1990	06-Nov-1990 to 14-Nov-1990	728

Note. SC = Southern California; NC = Northern California; OR = Oregon; and WA = Washington, with the numbering that orders the storms by their intensity for a given landfalling region. Two to three days of a spin-up and spin-down period are used during the downscaling of each AR.

Model longwave radiation scheme (Mlawer et al., 1997), Mellor-Yamada and Nakanishi-Niino level-2.5 surface and boundary layer scheme (Nakanishi & Niino, 2006), and the Kain-Fritsch (new Eta) cumulus scheme (Kain, 2004) for 27 and 9 km domains and the Noah-MP land surface model (Niu et al., 2011). In the innermost 3 km domain, cumulus parameterization has been turned off, as theoretically, it is only valid for parent grid sizes coarser than 9 km (Skamarock & Klemp, 2008). Spectral nudging was employed over the outer domain above the boundary layer to reduce drift between ERA-Interim forcing data and WRF's internal tendencies (von Storch et al., 2000), but not over the two inner high-resolution domains. This setup uses 44 vertical levels with model top pressure at 50 hPa, with a higher density of stacked vertical levels near the surface to improve the representation of lower-level processes.

We reemphasize that in the present study, we do not seek to extensively optimize across the numerous possible combinations of WRF parameterizations and domain-related parameters. Instead, we use the most recent version of the WRF model and implement a suite of parameterizations borrowed from recent AR-focused studies that themselves engaged in extensive parameterization choice validation. Hence, our parameterization selection is heavily informed by those that have been successfully used in previous California-based downscaling work (Leung & Qian, 2009; Hughes et al., 2014; Swain et al., 2015; Sun et al., 2016; Walton et al., 2017; Pontoppidan et al., 1271; Huang et al., 2018). Specifically, Hughes et al. (2014) successfully used the same radiation schemes, microphysics, cumulus, and boundary schemes as we used here to comprehensively study a single historical AR event. We also used the same radiation schemes, microphysics, and cumulus schemes as Pontoppidan et al. (1271), who demonstrated the largest gains in WRF-simulated precipitation accuracy occurred when horizontal model grid resolution increased from 9 to 3 km during an extreme orographic precipitation event. This latter study, in conjunction with Swain et al. (2015), informed our decision to use both a large domain and a 27 km-9 km-3 km nesting ratio. Initial testing during the present study further suggested that such a scaling from 27 to 3 km was indeed appropriate for downscaling ERA-Interim reanalysis and introduced no unexpected or unrealistic spatial discontinuities at the nested domain boundaries.

In our downscaling experiments, the 27 and 9 km outer domains are set to be quite large relative to those typically used in previous case study experiments, extending from southwest of the Hawaiian Islands to the eastern slopes of the Rocky Mountains. This is intended to accommodate the fact that ARs can exhibit a great spatial extent in length (2,000 km or longer) and a very narrow spatial extent in width (200–300 km or so). Additionally, the inner high-resolution 3 km domain extends relatively far west from the region of interest over the U.S. west coast, in order to relegate any potential boundary effects near the nested domain transition zones to regions away from the primary region of focus. This approach is motivated by Swain et al. (2015), who validated the performance of 4 km WRF using a large domain to simulate fine-scale features of ARs that were still well offshore.

We further note that the nested downscaling methodology we employ in the present study is not the only possible approach in investigating fine-scale extreme events. As computing power has increased and numerical model development has advanced rapidly over the past several years, global-scale modeling tools have improved to the point that high-resolution weather-scale simulations are now possible in certain cases including but not limited to variable resolution global models and nonhydrostatic high-resolution global models (Huang et al., 2016; Kramer et al., 2018; Leung et al., 2013; Satoh et al., 2017). To date, however, such methods have not been extensively validated with respect to the simulation of extreme AR-related precipitation events. Additionally, there remain a number of additional practical challenges, including (1) the ingestion of real-world (i.e., atmospheric reanalysis) boundary conditions using such frameworks as opposed to idealized or non-time-specific boundary conditions and (2) the still-daunting computational demands of large-scale nonhydrostatic modeling. Thus, high-resolution nested regional climate simulations, as implemented in this study, will remain an indispensable tool in the weather and climate community until such time that these cutting-edge alternative approaches reach maturity and available computational resources fully scale to the requisite level. We also note that statistical downscaling is an alternative approach for precipitation downscaling (Pierce et al., 2014). For example, Guirguis et al. (2019) recently assessed impacts of wetter/stronger ARs in a warming climate on fine-resolution precipitation over Western North America using statistical (Localized Constructed Analogs) downscaling of precipitation.

2.3. Investigating the Importance of Realistic Topographic Representation

A key goal of this study is to separately determine the effects of improved spatial resolution and other aspects of the high-resolution simulations on extreme AR characteristics. A second set of simulations is therefore conducted using the same downscaling framework described above, but using topography smoothed to the level appropriate for the 27 km domain. Differences in terrain between the native grid and the smoothed grid (hereafter smooth-topo) can be found in Figure S2. Substantial elevation differences are apparent, with either elevated mountains and lowered valleys in some regions along with general improvement of regional spatial details at 9 and 3 km. As a result, temperature, humidity, vertical motion, possible local circulations, and other associated dynamical and thermodynamic factors have the potential to be affected by the perturbed topography in this portion of the experiment.

2.4. Observational Data for Model Validation

To assess the performance of our model configuration and downscaling framework in capturing precipitation from landfalling ARs, we compare simulated precipitation to both in situ station observations and gridded observational data. In performing this validation, in situ station measurements are our best primary source data for evaluating extreme precipitation totals but are only available at a limited number of locations. We acknowledge that in situ observations are not without uncertainty themselves, with different aerial coverages between the grid-averaged precipitation estimates and the in situ observations at point scale. Meanwhile, gridded data sets offer a spatially complete picture, but they rely on interpolation algorithms to determine values away from stations. Since these interpolation algorithms often incorporate simplistic assumptions of how climate elements vary in space, the reliability of gridded data sets can be especially problematic in areas with sparse station data or complex terrain—as is the case across much of the Western United States (Henn et al., 2018; Walton & Hall, 2018). Thus, gridded data are used primarily for evaluating the spatial patterns of our WRF simulations but with the understanding that they represent a plausible estimate of what the true spatially complete field might have been.

The station observations used here are from the Global Historical Climatology Network Daily (GHCND) data set (Menne et al., 2012), and gridded data are from the daily 4 km data from the Parameter-elevation Relationships on Independent Slopes Model (PRISM; Daly et al., 2008). PRISM takes station measurements and applies a weighted regression scheme that accounts for many factors affecting the local climatology.

3. Results and Discussion

3.1. Water Vapor Transport

The large-scale IVT pattern over the northeastern Pacific is generally well captured by the high-resolution simulations (Figure 2), though the intensity and spatial orientation of each simulated AR still exhibit differences when compared to MERRA-2 data set (see Video S1). The positioning and shape of the simulated ARs are similar to the MERRA-2 high-resolution data set in both the 27 and 9 km simulations (see Video S1), which cover a large portion of the northeastern Pacific Ocean. As mentioned briefly in the experimental design section, previous work using in situ aircraft observations of six ARs over the northeastern Pacific demonstrated that MERRA tends to better capture the key large-scale and mesoscale features of such events than other reanalysis products (Ralph et al., 2012).

Specifically, Ralph et al. (2012) found that total water vapor transport in the best-three reanalyses including MERRA was within +/−7% of the observed transport and within 5% of the observed width. Thus, the observed spatiotemporal correspondence between MERRA and our 3 km WRF simulations is a good indication that the simulated ARs are correctly evolving and propagating across the large domain. Additionally, the finer resolution simulations at 9 and 3 km yield more detailed dynamical features than are present in the 27 km domain or in MERRA, including occasional double-IVT maxima and well-organized synoptic-scale cyclones (see Video S1 and Figure S3 for each individual storm's maximum IVT snapshot for WRF9/3 km and reanalysis). Realistic representation of both large-scale and mesoscale meteorological features provides initial confidence that a regional modeling framework similar to the one used in the present study is appropriate in further study of the associated precipitation extremes (Cannon et al., 2018).

We further find that IVT generally intensifies as resolution increases (see Table 2 for maximum IVT values across coastal grids at different model resolutions). IVT from WRF 3 km is +7% to +22% greater than the forcing data. While modest in magnitude, this increase in simulated IVT at high resolutions occurs across each

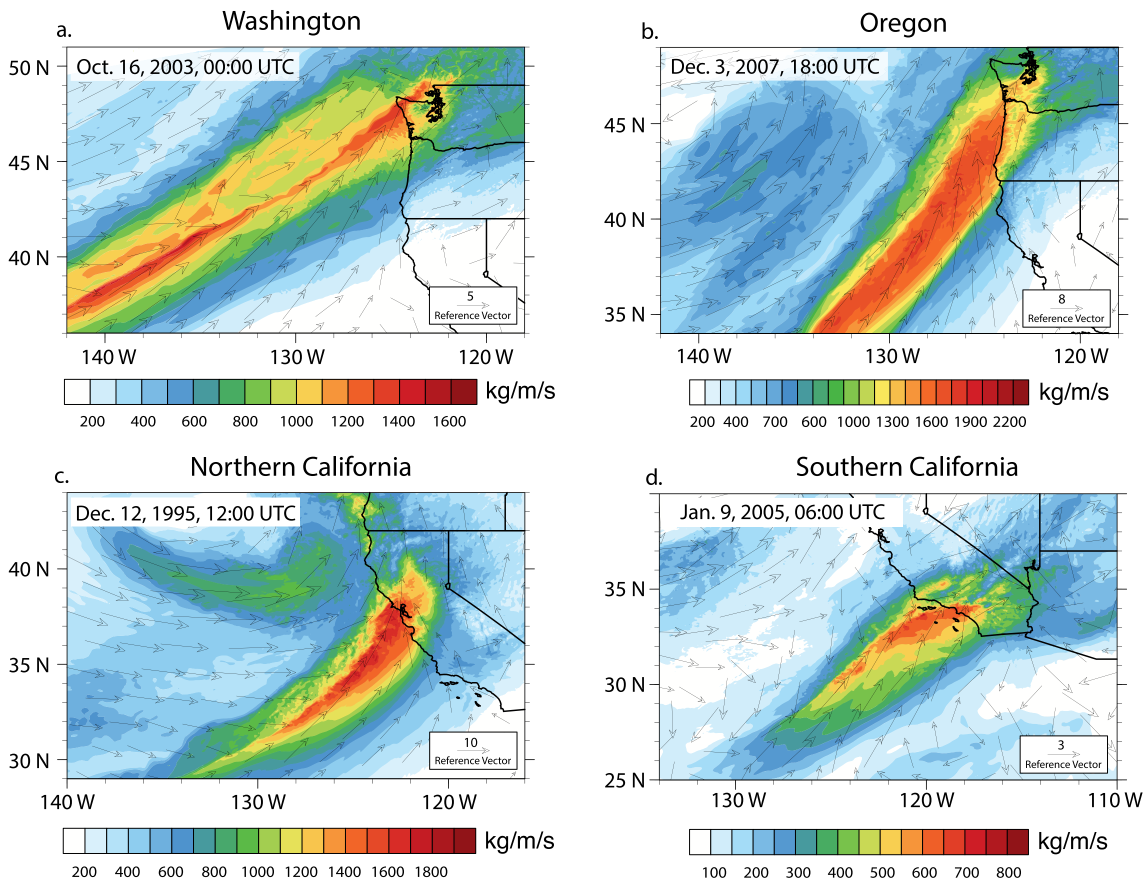

Figure 2. Simulated integrated vapor transport (IVT) (kg/m/s) from selected extreme AR events in each region. Instantaneous snapshot of IVT spatial patterns at the time of maximum water vapor transport (defined as 6-hourly maximum IVT at the nearest ocean gridbox). (Note: Fields are composed of 9 and 3 km WRF output, with 3 km superimposed upon 9 km where the 3 km domain spatially overlaps the 9 km domain.) Overlaid with near-surface (10 m) wind vectors (m/s).

Table 2
Maximum 6-Hourly Integrated Water Vapor Transport (IVT) for Each of the Nine Simulated AR Events Among the Near-Coast Grids

IVT (max)	ERA-interim	WRF 27 km	WRF 9 km	WRF 3 km
SC1	519	559	621	599
SC2	551	598	614	623
NC1	1,125	1,209	1,269	1,321
NC2	1,141	1,141	1,176	1,219
NC3	948	959	1,028	1,012
OR1	1,214	1,273	1,306	1,369
OR2	1,392	1,378	1,449	1,506
WA1	1,170	1,188	1,226	1,260
WA2	814	934	957	989

Note. Smoothed by daily running mean to reduce the timing variability from the instantaneous values (unit: kg/m/s). SC = Southern California; NC = Northern California; OR = Oregon; and WA = Washington.

of the nine events. Although direct comparison to in situ IVT observations was not possible for the events in this study, these findings are generally consistent with previous work demonstrating that high-resolution WRF simulations generate consistently larger and more accurate IVT extrema, relative to in situ aircraft observations obtained during the CALJET and PACJET campaigns, and then exist at the spatial resolution of parent forcing data sets (Swain et al., 2015).

3.2. Mean Versus Extreme Precipitation

To illustrate the value of multiscale downscaling using the chosen WRF configuration, we assess three main evaluation metrics, including (1) the spatial pattern of precipitation, (2) event-total precipitation for ARs in different landfall regions, and (3) localized precipitation maxima during individual events. We focus on three specific regions along the West Coast, each of which is characterized by mountainous terrain and high susceptibility to heavy precipitation: (1) the Olympic Peninsula and Northern Cascades (Olympics-Cascades), (2) the Sierra Nevada mountain range (Sierra Nevada), and (3) the Southern California Transverse Ranges (South CA). The precipitation for ARs making landfall near each region is shown in Figure 3a (also see Figure 4 for precipitation along the entire U.S. West Coast). The mean and maximum precipitation values in each of these three regions can also be found in Figure 3a. (Note that we have excluded relatively low [<20 mm per event] values from the area mean to focus on geographic regions that actually receive extreme precipitation.) For each of the three respective regions, only ARs making landfall within that region are included in model evaluations for each subregion. In addition to these regionally specific evaluations, we further use an overall performance metric assessing the simulated precipitation across all landfalling ARs included in the study.

Collectively, these side-by-side comparisons (Figure 3a) demonstrate a clear improvement in simulated mean precipitation spatially and quantitatively with finer resolution relative to PRISM, though with modest overall underestimation. Specifically, simulated event-total precipitation improves by 5–25% as resolution increases from 27 to 3 km in Olympics-Cascades and Southern CA, with overall good performance across resolutions in the Sierra Nevada, where mean biases are within 5% compared to PRISM. At higher resolutions (9 and 3 km), well-captured fine-scale precipitation spatial patterns are likely driven by highly localized topographical variations and associated orographic forcing effects, which are not present in either the reanalysis or 27 km model simulations. Details regarding topography can be found in Figure S4 for each respective data set and subregion.

More striking than these modest improvements in simulated mean AR precipitation, however, are the much larger and more systematic relative improvements in simulated extreme AR precipitation across all regions. Reduction in bias for event maximum precipitation values is as high as 40–60% in the finest 3 km simulations versus 27 km simulations (Figure 3a), relative to the PRISM data set. Precipitation maxima from WRF 3 km are close to those from PRISM (+/−15%). We do notice that peak simulated precipitation values (i.e., the maximum values shown in the Figure 3a) are slightly overestimated at 3 km by about 5% over the Sierra Nevada (Figure 3a), though these wet biases are still lower and less widespread than in previous studies of AR precipitation using WRF (e.g., Caldwell et al., 2009). An event-by-event comparison of precipitation between the forcing data set, finest-scale WRF output, and PRISM data can be found in Figure S5.

When using a uniform grid with WRF and PRISM regridded to 27 km (see Figure S6), the improvement in extreme precipitation from WRF 27 to 9 km (regridded to 27 km) or 3 km (regridded to 27 km) is around 20–50%, whereas the improvement was 40–60% on native grids. A significant portion of this reduction in bias likely stems from the explicit representation of mesoscale processes at higher resolutions in WRF including resolved convection at resolutions finer than 10 km (Sun et al., 2016; Walton et al., 2017). Further, accurate representation of complex topography is critically important in capturing the strong but highly localized vertical motion associated with orographic precipitation, as discussed further in section 3.3. Similar results are also found when regridding to the finer 4 km PRISM resolution, as shown in Figure S7.

Considering the uncertainty in gridded observations (here PRISM) especially over some sparsely sampled topographically complex regions, analyses of in situ data are also performed using GHCND station measurements. For the purpose of our focus on extreme precipitation, the top 1% of all available station values (i.e., the values above the 99th percentile of all the stations) during a given AR are selected and subsequently compared to corresponding ERA-interim, WRF, and PRISM values from the nearest grid points (Figure 3b). When restricting the analysis to only these wettest stations, the improvement compared to in situ data is even larger reaching as high as 70% as resolution increases from 9 to 3 km (up to 200% when from 27 to

10.1029/2019JD031554

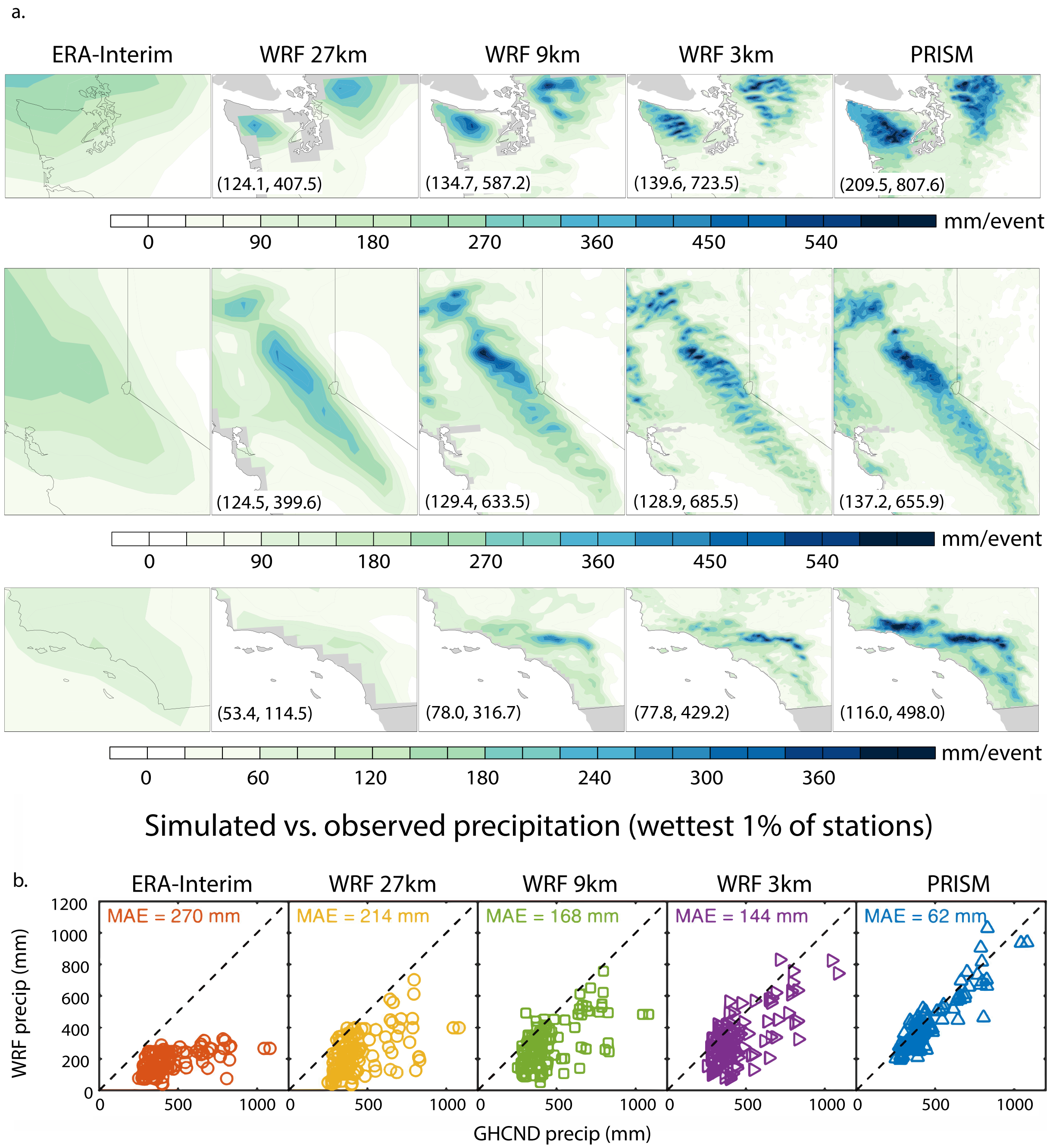

Figure 3. Simulated versus observed precipitation. (a) Event-total precipitation (mm/event) averaged over AR events making landfall along the subregions of U.S. West Coast from north to south, including Olympics-Cascades (two events), the Sierra Nevada (three events), and Southern California (two events) from ERA-Interim, WRF simulations, and PRISM. Pair values in the lower-left corner of each subpanel are average and maximum grid box precipitation values, respectively, taken from the subregion domains. (b) Simulated versus observed accumulated total precipitation for the wettest 1% of GHCND stations for each AR event (the scatter points include the values from all of the nine events). Mean absolute error (MAE) is reported in the upper part of each panel.

3 km) for the simulated event-total precipitation over stations. On average, ERA-Interim has the highest mean absolute error (MAE) (270 mm), while WRF has lower MAE values that decrease monotonically from 27, 9, to 3 km resolutions (214, 168, and 144 mm, respectively). PRISM has the lowest MAE (66 mm), which reflects the fact that PRISM incorporates the GHCND data into its interpolation scheme and thus should be expected to match the station data most closely. We note that these results are insensitive to the regridding approach used (i.e., uniform regridding to either coarse or fine grid, as previously discussed).

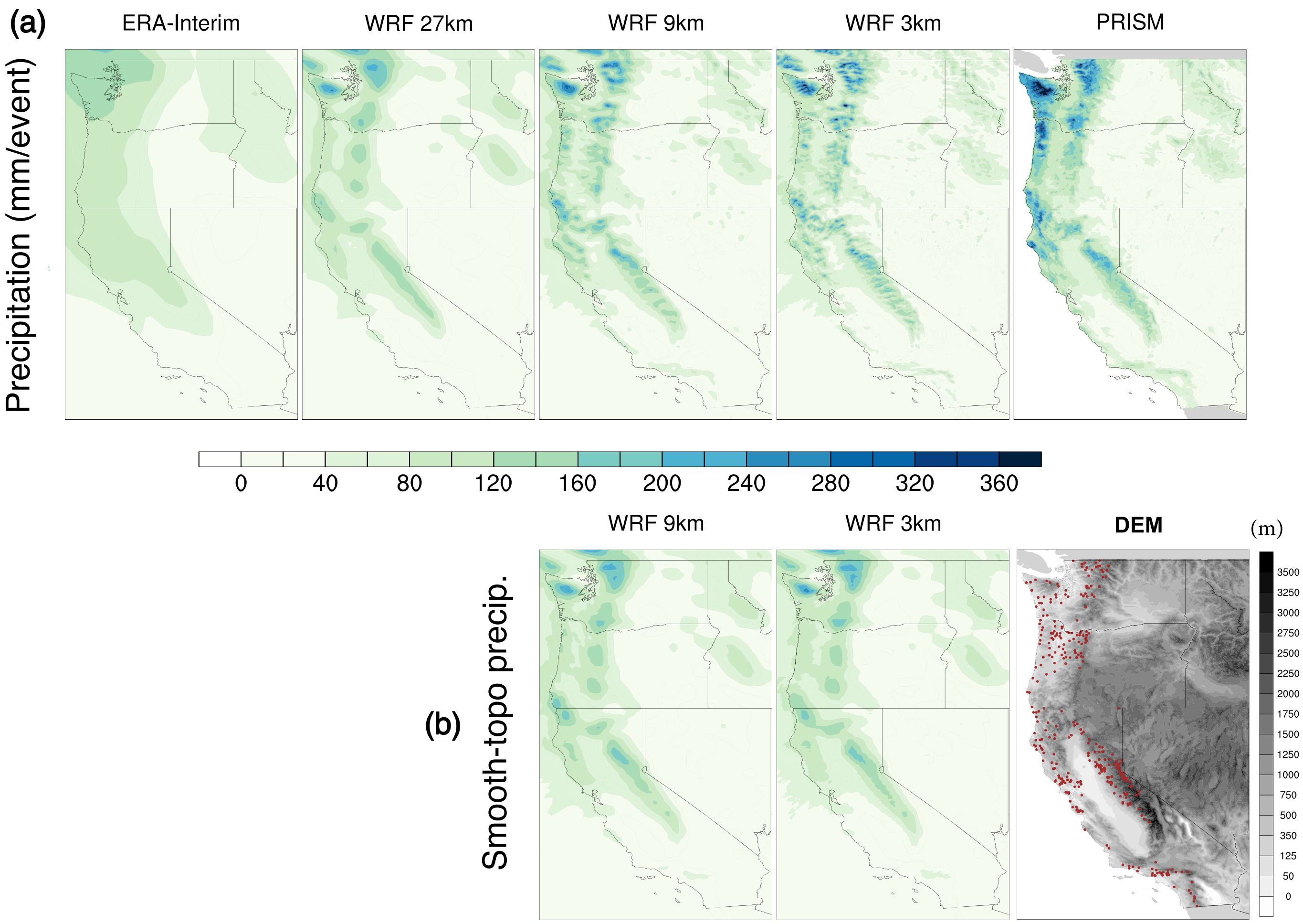

Figure 4. Event-total AR precipitation at native resolution for different data sets. (a) Event-total precipitation (mm/event) averaged over nine extreme ARs making landfall along the U.S. West Coast in ERA-Interim, WRF simulations, and PRISM; (b) similar as (a) but for the precipitation at 9 and 3 km from the smooth-topo set of simulations. The spatial distributions of the GHCND stations with event-total precipitation above 200 mm are depicted at the rightmost panel of section (b) with the elevation from PRISM overlaid.

We acknowledge the difficulties in quantifying uncertainties arising from the comparison between point-wise measurements and grid box values, as well as those stemming from different observational sources in complex terrain, where the elevation and associated orographically forced precipitation can vary greatly over a range of even a few kilometers. Additionally, gauges for the station observations are generally not located at the highest elevations across mountain chains, as they are often physically difficult to access and maintain. This means that true real-world regional precipitation maxima likely remain undersampled. Overall, WRF at 3 km generally yields the closest match with the PRISM data set, although WRF at 9 km can be also competitive with 3 km simulations, particularly in NC and in areas receiving very heavy precipitation (see comparable MAE and 1% precipitation values in Figure 3b). For the subset of very extreme AR events as studied here, 3 km WRF tends to systematically underestimate overall spatially averaged precipitation by ~5% to 30%, depending on subregion, in the wettest regions, suggesting that modeling limitations remain even at very high resolutions and may not be entirely solvable by increased model resolution of orographic processes.

In addition to the spatial features discussed above, we have also analyzed the temporal evolution of simulated precipitation in WRF. To do so, we generate time series of precipitation accumulation using data regridded to the same resolution as PRISM (see Figure 5) in order to make an apples to apples comparison across different spatial grids. We emphasize that we focus specifically on the regions of most intense precipitation and have selected the regions with event-total precipitation above certain thresholds (≥200 mm for SC and ≥300 mm elsewhere)—to investigate the effect of resolution on the areas most heavily affected by these

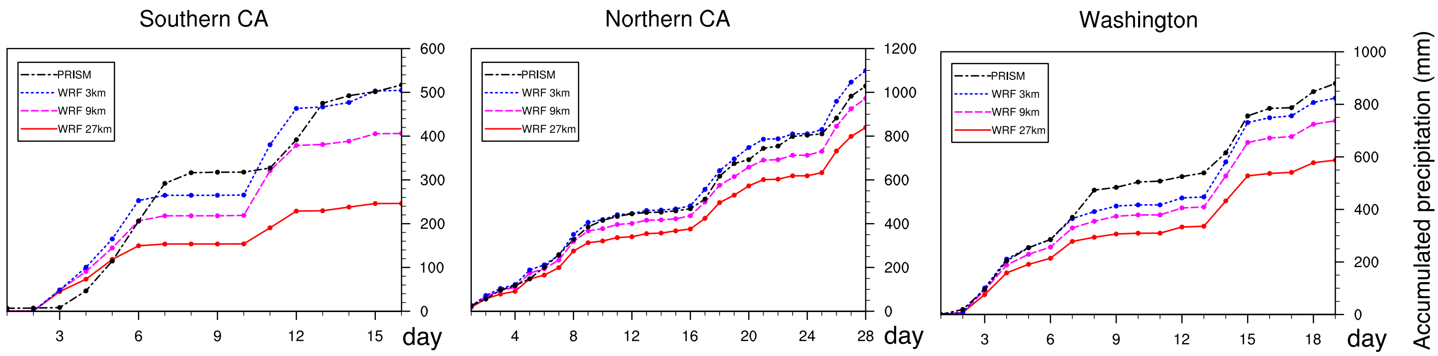

Figure 5. Time series of precipitation accumulation (mm) using WRF data regridded to the PRISM (4 km) grid. Grid boxes with event-total precipitation above certain thresholds are selected and averaged for each of the three regions to focus specifically upon the geographically limited regions experiencing the most extreme precipitation during these events (using thresholds of ≥200 mm for SC and ≥300 mm for all other regions). We show the day-to-day sequence of the precipitation accumulated from all of the AR events in each region.

intense landfalling ARs. Nonetheless, the findings are generally insensitive to different thresholds for this temporal analysis. Using daily accumulated precipitation as a metric from the targeted events in each of the three regions (i.e., day-to-day sequence of the precipitation accumulated from the AR events in each region), we find that WRF at its finest scale yields the most accurate cumulative precipitation traces in all study regions, with corresponding biases of +/−15% or less for all four subregions. Progressively coarser resolution simulations yield progressively greater underestimation of accumulated precipitation over time. WRF at its coarsest scale 27 km underestimates the precipitation accumulation above the threshold by about 50%, 20%, and 33% over the SC, NC, and WA regions, respectively, relative to PRISM data. WRF at 9 km shows significant improvement relative to 27 km but still underestimates daily-accumulated precipitation by about 20%, 5%, and 15% over the respective regions relative to PRISM. Notably, precipitation time series from WRF generally match the observed day-to-day sequence of temporal evolution at all resolutions.

3.3. Sensitivity of Simulated Precipitation to Terrain Smoothing

To quantify the contribution of improvement in simulated extreme precipitation at higher model spatial resolutions that is directly attributable to better-resolved topography, we conduct additional experiments using topographical boundary conditions smoothed to 27 km resolution but preserving high atmospheric resolution for all the domains. We present side-by-side comparisons of the smooth-topo simulations and native-grid simulations (Figure 6a). We find that the smooth-topo simulations yield similar spatial patterns, with only a slight improvement in aerially averaged precipitation compared to PRISM (see Figure 3a), ranging from ~1% in WA to 10% in SCA when resolution increases from 27 to 3 km (Figure 6a). We note similar improvements in domain maximum precipitation, ranging from 5% in WA to as high as 13% in SCA of which occurs between 27 and 9 km (with little further improvement from 9 to 3 km; cf. left/center, center/right panels of Figure 6a). Relative to PRISM, the overall bias in simulated precipitation remains fairly large for both mean (10% to 50%) and extreme values (30% to 65%) (referring to the values in the lower-left corner of each subpanel including area mean and area maximum) at all smooth-topo resolutions in different regions.

To further illustrate the importance of finely resolved topography as opposed to the effect of increased spatial resolution within the model itself, we conduct a gridbox-scale analysis of the difference between precipitation in the smooth-topo versus native resolution simulations (see scatter plot in Figure 6b). We find a striking divergence between the smoothed topography versus native topography at more extreme precipitation values in each region—an effect that is especially apparent at 3 km resolution. In general, simulations using finely resolved topography yield much more intense precipitation maxima than do simulations using coarsened topography, despite more muted changes for less intense precipitation. In particular, we report far more gridboxes receiving extreme precipitation (using a 400 mm/event threshold across more northern regions), ranging from a 50–500% increase (see the points outside the dashed lines in Figure 6b) from smoothed to native topography—even at the same model resolution. Over the relatively drier SC region, the number of gridboxes exceeding 200 mm per event increases by a full order of magnitude (also see the points outside the dashed lines in Figure 6b) in the native grid relative to the smooth-topo simulations (Figure 6b, bottom). Since WRF generally underestimates precipitation extremes relative to observations, this suggests that

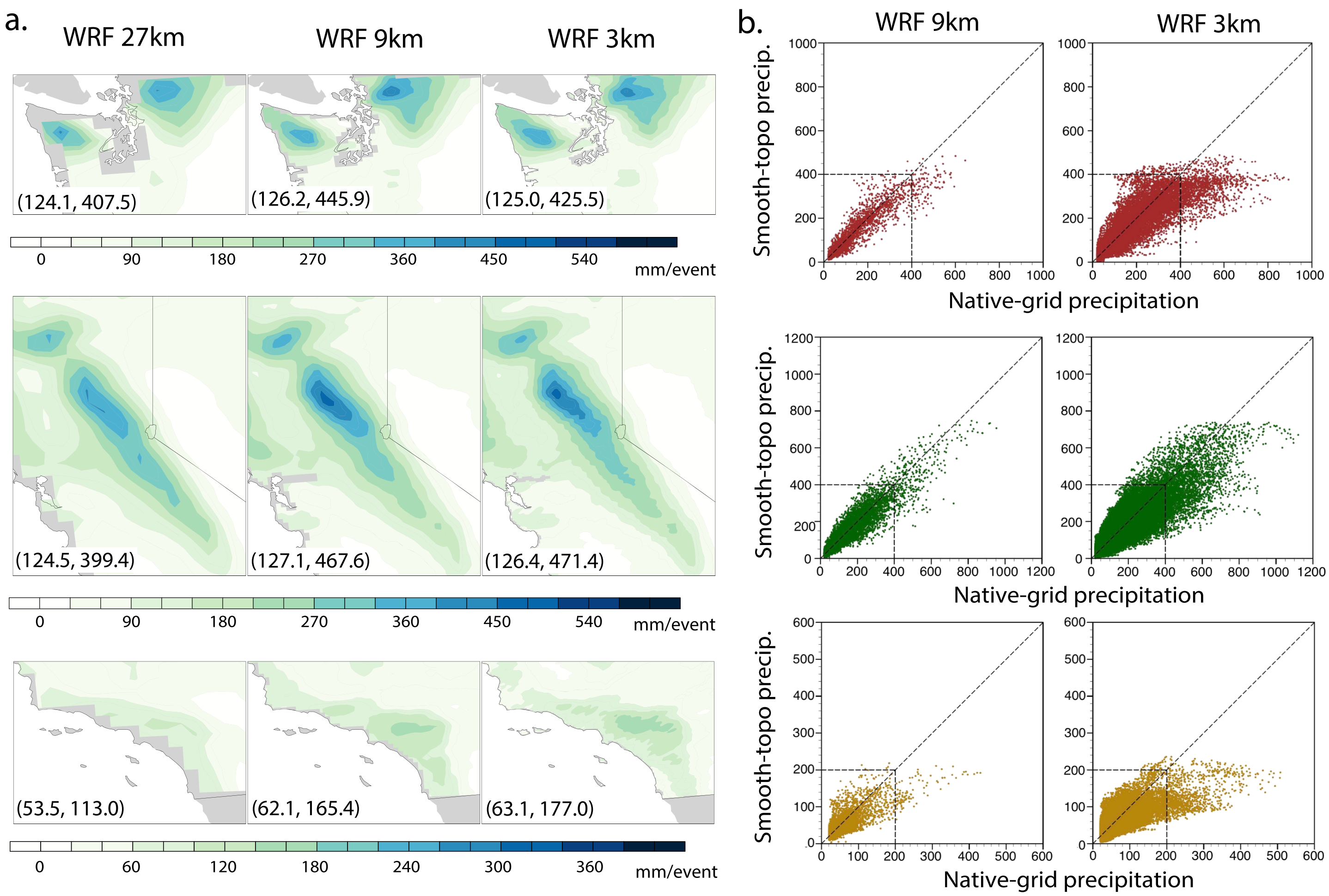

Figure 6. Smooth-topo versus native grid extreme AR precipitation. (a) Same as Figure 3a but for the output from smooth-topo simulations. (b) Smoothed topography versus native-grid accumulated total precipitation for all of the AR events over each region. Note: (1) The scatter points include grid-box values with event-total above 20 mm from corresponding ARs; (2) $y = x$ line is also depicted as a visual aid; and (3) dashed lines at certain thresholds are also added for better illustration.

a majority (85%) of the previously noted improvement with increased resolution does indeed come directly from the inclusion of finely resolved topography.

3.4. Vertical Motion, Extreme Winds, and Static Stability

While we find that the majority of spatially aggregated gains in simulated precipitation accuracy are derived by the increase in model resolution from 27 to 9 km, we have previously shown that the highest-resolution iteration of the model is critical in capturing the extreme precipitation values overall (Figure 3b). To further illustrate the importance of finer-scale resolution in capturing the underlying physical processes responsible for these extremes, we conduct a focused case study analysis using the 12 December 1995 AR event. This storm brought not only intense precipitation but also extremely strong winds to portions of NC, including gusts over 44.7 m/s (100 mph) in the coastal hills in the San Francisco Bay Area (Burt, 2007). The event was also characterized by an unusual amount of convective instability for a cool-season system along the Pacific Coast of North America, which may partially account for the degree of wind damage and flash flooding that ultimately occurred. We emphasize that we do not attempt to assess the absolute accuracy of WRF's representation of fine-scale phenomena given the lack of in situ or remotely sensed observations for the physical variables (wind profiles, vertical motions, and water vapor profiles) under consideration. Instead, we include the 12 December 1995 event as an illustrative example of how several precipitation-relevant physical variables vary in a spatiotemporal sense at different horizontal model resolutions given atmospheric boundary conditions that produce an especially powerful storm event in WRF. In particular, we seek to determine whether certain specific phenomena, known to be critical for the generation of extreme precipitation during AR events, only emerge when the horizontal resolution of WRF is high.

We first construct height-longitude transects bisecting the AR near the point of landfall in the San Francisco Bay Area, extending from the Pacific Ocean west of San Francisco (in the cool sector), across the Central Valley (within the warm sector) to the eastern (lee)side of the Sierra Nevada Mountains. Examining the spatial variation of atmospheric vertical motion across these transects, several features of interest become apparent. We find that the magnitude and sign of vertical motion (W) is strongly associated with topography, as expected (Figures 7a–7c). Given the prevailing southerly wind across the domain in advance of the strong offshore cold front (Figure 2c), south facing slopes are generally orthogonal to the mean wind direction and are therefore experiencing upslope winds and hence orographically forced upward vertical motion (Figure 7d). The spatial pattern of W is greatly smoothed at coarser resolutions of 27 and 9 km, with much sharper horizontal and vertical gradients apparent in the 3 km simulation. For each tripling of resolution (i.e., from 27 to 9 km or 9 to 3 km), we report an approximate doubling in the mean W, which is positive in each case, and an approximate quadrupling in the magnitude of both maximum upward and maximum downward motion (Figure 7a–7c). These striking differences illustrate the importance of high resolution in capturing orographic forcing that is intimately tied to the generation of precipitation extremes and suggest a possible mechanism for the extreme precipitation accuracy gains observed at the highest 3 km model resolution. Previous work has more extensively discussed these factors, including the orientation of topography relative to impinging airflow, orographic/vertical uplift, and the role of mean versus anomalous wind fields in this region) (Dettinger et al., 2004; Huning & Margulis, 2018; Lundquist et al., 2010; Neiman et al., 2013; Smith, 1979).

We note that WRF's depiction of strong simulated vertical motion in the vicinity of complex topography may be the result of vertically propagating gravity waves. WRF's representation of topographically forced gravity waves is highly sensitive to vertical as well as horizontal resolution (Miglietta & Rotunno, 2005), which complicates the interpretation of the role of these alternating bands of upward/downward motion. Pontoppidan et al. (1271) studied an intense precipitation event in complex terrain using WRF with similar parameterization settings as in our study, finding that 3 km grid spacing was adequate to represent important dynamical features such as gravity waves due to the resolution of shorter wavelength phenomena but that 9 km spacing was insufficient to do so. Nevertheless, we emphasize that substantial differences between the 3 km and 9/27 km simulations exist even in regions unaffected by topographically generated gravity waves over the Pacific Ocean.

Additionally, the 3 km WRF simulation generates a narrow but intense region of upward vertical motion on the western margin of the AR just ahead of the cold front. This region is on the margin of the higher CAPE region and is spatially coincident with the strongest near-surface winds (Figures 7d vs. 7e), as detailed below. The discontinuous but broadly linear structure of this band strongly suggests that it may be associated with a narrow cold frontal rainband (Cannon et al., 2018). These occasional features of West Coast ARs have recently been associated with high-impact storm-related hazards (e.g., the deadly Montecito debris flow in January 2018; Oakley et al., 2018). Notably, this narrow cold frontal rainband-like feature is absent in the 9 and 27 km simulations (Figures 7a vs. 7b and 7c) suggesting that the 3 km resolution is important in capturing unusual physical phenomena that can occur within or near the AR environment during intense storm events.

As previously mentioned, the December 1995 event was characterized by powerful surface winds and a modest amount of convective instability. Low static stability is unusual in West Coast AR environments, which are typically characterized by moist-neutral vertical profiles (e.g., Neiman et al., 2008; Ralph et al., 2004). In this case, we find that the 3 km WRF simulation captures both of these anomalous characteristics, generating very strong winds within the boundary layer nearing hurricane force 60 m above ground level, and elevated convective available potential energy (CAPE; Figure 7f). During this event, simulated CAPE locally exceeds 200 J/kg, which is low in absolute terms but relatively high by local standards. Indeed, Oakley et al. (2017) find that the median CAPE during historical California ARs that produced extreme precipitation leading to debris flows was only on the order of 20–40 J/kg in cyclonic warm sector preceding cold frontal passage. Moreover, Monteverdi et al. (2003) find that low CAPE environments (200–400 J/kg) were typical even during tornadic thunderstorm events in this region—whereas much higher values (2,000 J/kg or

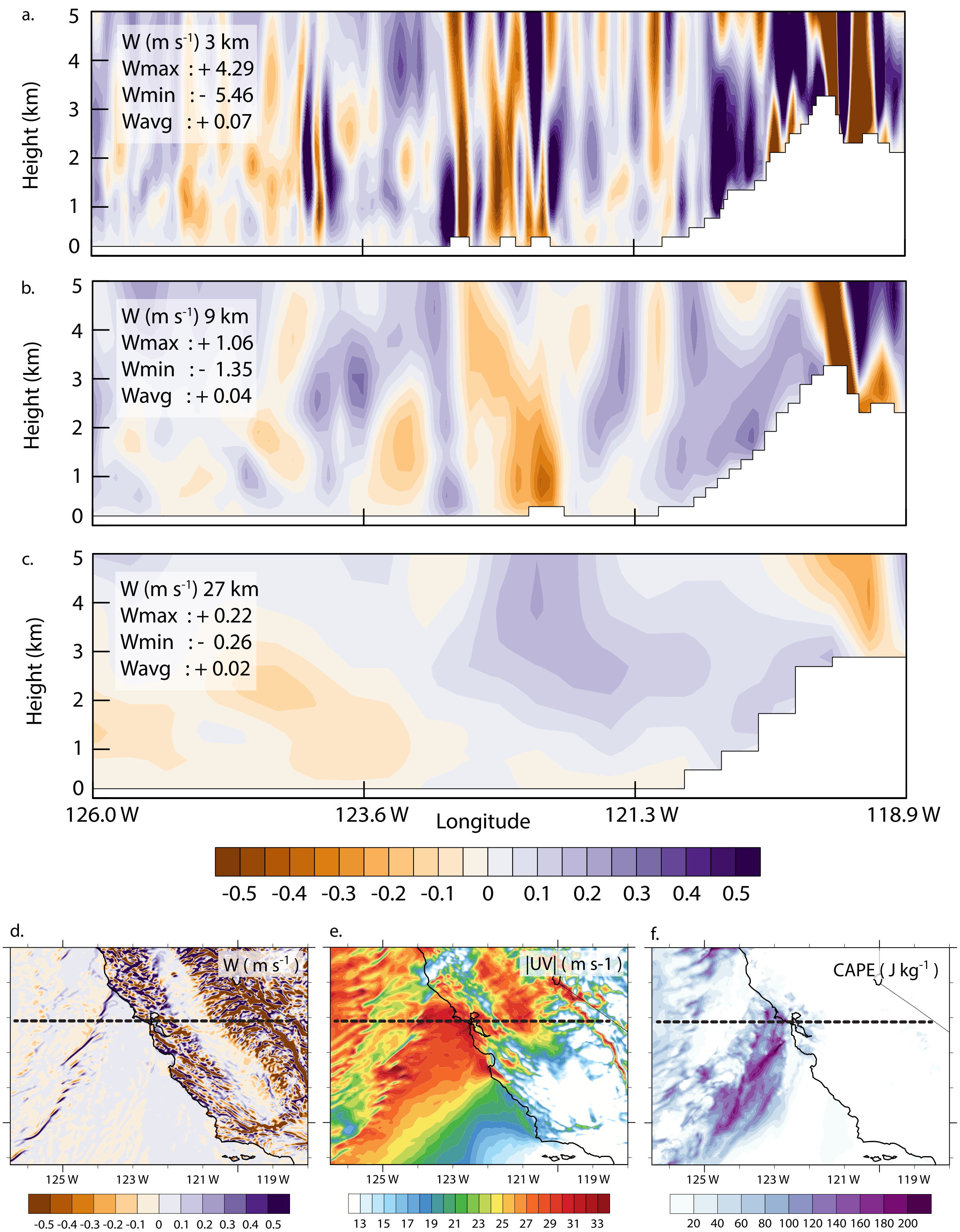

Figure 7. Snapshot of fine-scale spatial characteristics of extreme AR event on 12 December 1995 (11:00 UTC). Cross section (126–118.5° W at 37.9° N), transect shown in panels (d)–(f). (a) Vertical velocity in the lowest 5 km of the atmosphere (W; m/s) within the 3 km WRF nest. Quantities noted in the inset box are the maximum, minimum, and average values for W within the cross section. White masking represents the height of local topography. (b and c) Same as (a) but for the 9 and 27 km WRF nests, respectively. (d) Map view of near-surface vertical motion (fifth model vertical level, 230 m above local topography) for the 3 km WRF output. (e) Near-surface wind speed for the 3 km WRF output (second model vertical level, 60 m above local topography, m/s). Note that 33 m/s (74 mph) is equivalent to hurricane force. (f) Convective available potential energy (CAPE) at the surface for the 3 km WRF output.

more) are more typical of severe convective events elsewhere in North America. Thus, taking into account this detail of regional climatology, we suggest that the existence of CAPE >200 J/kg can potentially be an important thermodynamic differentiator when it comes to AR impacts along the California coast.

4. Discussion and Conclusions

In this study, a targeted selection of the most intense historical AR events making landfall on the West Coast of the United States are selected using an object-oriented AR detection approach. We dynamically downscale these events, using nested WRF simulations at 27, 9, and 3 km forced by the ERA-Interim reanalysis, to examine extreme precipitation and other relevant fine-scale thermodynamic and kinematic quantities event by event. Previous studies suggest resolutions of ~10 km are needed to capture realistic orographic precipitation processes in mountainous regions (Minder et al., 2016; Pavelsky et al., 2012; Rasmussen et al., 2011; Wrzesien et al., 2017). Our results reinforce these earlier findings but also provide substantial additional insights into the importance of fine spatial resolution in the representation of precipitation and water vapor transport extrema—as well as resolution-dependent drivers in topographically complex regions.

We find that the simulations resulting from this modeling framework (1) can reproduce the localized, filamentary corridors of integrated vapor transport (IVT) characteristic of extreme AR events; (2) can capture precipitation associated with these strong ARs, most notably the extreme precipitation in topographically complex regions from the finest-scale output; and 3) can capture fine-scale physical phenomena such as orographically forced vertical motion, strong low-level wind speeds, and convective instability. We demonstrate that high horizontal resolution—finer than 10 km—is especially important in capturing localized AR precipitation maxima and results in greater than 50% improvement in the simulation of these precipitation extremes relative to coarser simulations using the same model. We further show that a majority (~85%) of the gains in accuracy in simulated extreme precipitation with increased model resolution accrue due to enhanced resolution of the topographical boundary conditions—highlighting the importance of orographic processes in producing localized regions of extreme precipitation accumulation during AR events.

These findings highlight the importance of better-resolved fine-scale processes in capturing AR-related precipitation extremes. Broad-scale spatial features, such as the placement of parent cyclones and the orientation of IVT corridors, are well represented even in the coarser spatial resolution simulations. However, the ability to capture the fine-scale spatial features most relevant for AR-related natural hazard impacts, for example, flooding, mudslides or debris flows, and wind damage, appears to be limited to higher-resolution at 3 km simulations. Collectively, these results demonstrate that high-resolution simulations are not only an effective tool for studying ARs in general but are also necessary to capture extrema of various meteorological quantities that produce many of the natural hazards associated with these events. Moving forward, high-resolution simulations have the potential to provide watershed-specific projections of extreme precipitation that will have considerable relevance across a wide range of timescales—from short-term forecast-informed reservoir operations to long-term climate adaptation activities.

Acknowledgments
We sincerely thank the reviewers for their insightful comments on our manuscript. The authors thank J. David Neelin for his generous computational support. Thanks also go to Neil Berg for his helpful suggestions. We acknowledge the substantial efforts behind the PRISM gridded observation data set and the station measurements GHCND used in this study. Data used in the study can be accessed through the public link http://portal.nersc.gov/project/m2637/ARs or by contacting the corresponding author (at xingyhuang@gmail.com). This research was funded by the U.S. Department of Energy, Office of Science, projects An Integrated Evaluation of the Simulated Hydroclimate System of the Continental US (Award DE-SC0016605), A Hierarchical Evaluation Framework for Assessing Climate Simulations Relevant to the Energy-Water-Land Nexus (Award DE-SC0016438), and Developing Metrics to Evaluate the Skill and Credibility of Downscaling (Award DE-SC0014061). D. L. S. was supported by a joint collaboration between the Institute of the Environment and Sustainability at the University of California, Los Angeles; the Center for Climate and Weather Extremes at the National Center for Atmospheric Research; the Nature Conservancy of California; and UCLA's Sustainable LA Grand Challenge.

References

Burt, C. C. (2007). *Extreme weather: A guide and record book*: WW Norton & Company.

Caldwell, P., Chin, H.-N. S., Bader, D. C., & Bala, G. (2009). Evaluation of a WRF dynamical downscaling simulation over California. *Climate Change*, *95*(3-4), 499–521.

Cannon, F., Hecht, C. W., Cordeira, J. M., & Ralph, F. M. (2018). Synoptic and mesoscale forcing of Southern California extreme precipitation. *Journal of Geophysical Research: Atmospheres*, *123*, 13,714–13,730. https://doi.org/10.1029/2018JD029045

Chen, X., Leung, L. R., Gao, Y., Liu, Y., Wigmosta, M., & Richmond, M. (2018). Predictability of extreme precipitation in western US watersheds based on atmospheric river occurrence, intensity, and duration. *Geophysical Research Letters*, *45*, 11,693–11,701. https://doi.org/10.1029/2018GL079831

Daly, C., Halbleib, M., Smith, J. I., Gibson, W. P., Doggett, M. K., Taylor, G. H., et al. (2008). Physiographically sensitive mapping of climatological temperature and precipitation across the conterminous United States. *International Journal of Climatology*, *28*(15), 2031–2064.

Dee, D., Uppala, S., Simmons, A., Berrisford, P., Poli, P., Kobayashi, S., et al. (2011). The ERA-interim reanalysis: Configuration and performance of the data assimilation system. *Quarterly Journal of the Royal Meteorological Society*, *137*(656), 553–597.

Dettinger, M. D., Ralph, F. M., Das, T., Neiman, P. J., & Cayan, D. R. (2011). Atmospheric rivers, floods and the water resources of California. *Water*, *3*(2), 445–478.

Dettinger, M., Redmond, K., & Cayan, D. (2004). Winter orographic precipitation ratios in the Sierra Nevada—Large-scale atmospheric circulations and hydrologic consequences. *Journal of Hydrometeorology*, *5*(6), 1102–1116.

Dominguez, F., Rivera, E., Lettenmaier, D., & Castro, C. (2012). Changes in winter precipitation extremes for the western United States under a warmer climate as simulated by regional climate models. *Geophysical Research Letters*, *39*, L05803. https://doi.org/10.1029/2011GL050762

Dudhia, J. (1989). Numerical study of convection observed during the winter monsoon experiment using a mesoscale two-dimensional model. *Journal of the atmospheric sciences*, *46*(20), 3077–3107.

Eldardiry, H., Mahmood, A., Chen, X., Hossain, F., Nijssen, B., & Lettenmaier, D. P. (2019). Atmospheric river-induced precipitation and snowpack during the western United States cold season. *Journal of Hydrometeorology*, *20*(4), 613–630.

Espinoza, V., Waliser, D. E., Guan, B., Lavers, D. A., & Ralph, F. M. (2018). Global analysis of climate change projection effects on atmospheric rivers. *Geophysical Research Letters*, *45*, 4299–4308. https://doi.org/10.1029/2017GL076968

Field, C. B., Barros, V., Stocker, T. F., & Dahe, Q. (2012). *Managing the risks of extreme events and disasters to advance climate change adaptation: Special report of the intergovernmental panel on climate change*. Cambridge: Cambridge University Press.

Gao, Y., Lu, J., Leung, L. R., Yang, Q., Hagos, S., & Qian, Y. (2015). Dynamical and thermodynamical modulations on future changes of landfalling atmospheric rivers over western North America. *Geophysical Research Letters*, *42*, 7179–7186. https://doi.org/10.1002/2015GL065435

Gershunov, A., Shulgina, T., Ralph, F. M., Lavers, D. A., & Rutz, J. J. (2017). Assessing the climate-scale variability of atmospheric rivers affecting western North America. *Geophysical Research Letters*, *44*, 7900–7908. https://doi.org/10.1002/2017GL074175

Guan, B., & Waliser, D. E. (2015). Detection of atmospheric rivers: Evaluation and application of an algorithm for global studies. *Journal of Geophysical Research: Atmospheres*, *120*, 12,514–12,535. https://doi.org/10.1002/2015JD024257

Guirguis, K., Gershunov, A., Shulgina, T., Clemesha, R. E., & Ralph, F. M. (2019). Atmospheric rivers impacting Northern California and their modulation by a variable climate. *Climate Dynamite*, *52*(11), 6569–6583.

Henn, B., Newman, A. J., Livneh, B., Daly, C., & Lundquist, J. D. (2018). An assessment of differences in gridded precipitation datasets in complex terrain. *Journal of Hydrology*, *556*, 1205–1219.

Huang, X., Hall, A. D., & Berg, N. (2018). Anthropogenic warming impacts on today's Sierra Nevada snowpack and flood risk. *Geophysical Research Letters*, *45*, 6215–6222. https://doi.org/10.1029/2018gl077432

Huang, X., Rhoades, A. M., Ullrich, P. A., & Zarzycki, C. M (2016). *An evaluation of the variable resolution-CESM for modeling California's climate* (Vol. 8, pp. 345–369). https://doi.org/10.1002/2015MS000559

Huang, X., & Ullrich, P. A. (2017). The changing character of 21st century precipitation over the western United States in the variable-resolution CESM. *Journal Climate*, *30*(18), 7555–7575.

Hughes, M., Mahoney, K. M., Neiman, P. J., Moore, B. J., Alexander, M., & Ralph, F. M. (2014). The landfall and inland penetration of a flood-producing atmospheric river in arizona. Part II: Sensitivity of modeled precipitation to terrain height and atmospheric river orientation. *Journal of Hydrometeorology*, *15*(5), 1954–1974.

Huning, L. S., & Margulis, S. A. (2018). Investigating the variability of high-elevation seasonal orographic snowfall enhancement and its drivers across sierra nevada, california. *Journal of Hydrometeorology*, *19*(1), 47–67.

Jackson, D. L., Hughes, M., & Wick, G. A. (2016). Evaluation of landfalling atmospheric rivers along the US West Coast in reanalysis data sets. *Journal of Geophysical Research: Atmospheres*, *121*, 2705–2718. https://doi.org/10.1002/2015JD024412

Kain, J. S. (2004). The Kain-Fritsch convective parameterization: an update. *Journal of Applied Meteorology and Climatology*, *43*(1), 170–181.

Kim, J., Guan, B., Waliser, D., Ferraro, R., Case, J., Iguchi, T., et al. (2018). Winter precipitation characteristics in western US related to atmospheric river landfalls: Observations and model evaluations. *Climate Dynamite*, *50*(1-2), 231–248.

Konrad, C. P., & Dettinger, M. D. (2017). Flood runoff in relation to water vapor transport by atmospheric rivers over the western United States, 1949–2015. *Geophysical Research Letters*, *44*, 11,456–11,462. https://doi.org/10.1002/2017GL075399

Kramer, M., Heinzeller, D., Hartmann, H., van den Berg, W., & Steeneveld, G.-J. (2018). Assessment of MPAS variable resolution simulations in the grey-zone of convection against WRF model results and observations. *Climate Dynamite*, *2018*, 1–24.

Leung, L. R., Mearns, L. O., Giorgi, F., & Wilby, R. L. (2003). Regional climate research: Needs and opportunities. *Bulletin of the American Meteorological Society*, *84*(1), 89–95. https://doi.org/10.1175/BAMS-84-1-89

Leung, L. R., & Qian, Y. (2009). Atmospheric rivers induced heavy precipitation and flooding in the western US simulated by the WRF regional climate model. *Geophysical Research Letters*, *36*, L03820. https://doi.org/10.1029/2008GL036445

Leung, L. R., Ringler, T., Collins, W. D., Taylor, M., & Ashfaq, M. (2013). A hierarchical evaluation of regional climate simulations, Eos. *Transactions American Geophysical Union*, *94*(34), 297–298.

Lundquist, J. D., Minder, J. R., Neiman, P. J., & Sukovich, E. (2010). Relationships between barrier jet heights, orographic precipitation gradients, and streamflow in the northern Sierra Nevada. *Journal of Hydrometeorology*, *11*(5), 1141–1156.

Martin, A., Ralph, F. M., Demirdjian, R., DeHaan, L., Weihs, R., Helly, J., et al. (2018). Evaluation of atmospheric river predictions by the WRF model using aircraft and regional mesonet observations of orographic precipitation and its forcing. *Journal of Hydrometeorology*, *19*(7), 1097–1113.

Mass, C. F., Ovens, D., Westrick, K., & Colle, B. A. (2002). Does increasing horizontal resolution produce more skillful forecasts? The results of two years of real-time numerical weather prediction over the Pacific Northwest. *Bulletin of the American Meteorological Society*, *83*(3), 407–430.

Menne, M. J., Durre, I., Vose, R. S., Gleason, B. E., & Houston, T. G. (2012). An overview of the Global Historical Climatology Network Daily database. *Journal of Atmospheric and Oceanic Technology*, *29*(7), 897–910.

Miglietta, M., & Rotunno, R. (2005). Simulations of moist nearly neutral flow over a ridge. *Journal of the Atmospheric Sciences*, *62*(5), 1410–1427.

Minder, J. R., Letcher, T. W., & Skiles, S. M. (2016). An evaluation of high-resolution regional climate model simulations of snow cover and albedo over the Rocky Mountains, with implications for the simulated snow-albedo feedback. *Journal of Geophysical Research: Atmospheres*, *121*, 9069–9088. https://doi.org/10.1002/2016JD024995

Mlawer, E. J., Taubman, S. J., Brown, P. D., Iacono, M. J., & Clough, S. A. (1997). Radiative transfer for inhomogeneous atmospheres: RRTM, a validated correlated-k model for the longwave. *Journal of Geophysical Research*, *102*(D14), 16,663–16,682.

Monteverdi, J. P., Doswell, IIIC. A., & Lipari, G. S. (2003). Shear parameter thresholds for forecasting tornadic thunderstorms in northern and central California. *Weather and forecasting*, *18*(2), 357–370.

Nakanishi, M., & Niino, H. (2006). An improved Mellor–Yamada level-3 model: Its numerical stability and application to a regional prediction of advection fog. *Boundary-Layer Meteorology*, *119*(2), 397–407.

Nash, D., Waliser, D., Guan, B., Ye, H., & Ralph, M. (2018). The role of atmospheric rivers in extratropical and polar hydroclimate. *Journal of Geophysical Research: Atmospheres*, *123*, 6804–6821. https://doi.org/10.1029/2017JD028130

Neiman, P. J., Hughes, M., Moore, B. J., Ralph, F. M., & Sukovich, E. M. (2013). Sierra barrier jets, atmospheric rivers, and precipitation characteristics in Northern California: A composite perspective based on a network of wind profilers. *Monthly Weather Review*, *141*(12), 4211–4233.

Neiman, P. J., Ralph, F. M., Wick, G. A., Lundquist, J. D., & Dettinger, M. D. (2008). Meteorological characteristics and overland precipitation impacts of atmospheric rivers affecting the West Coast of North America based on eight years of SSM/i satellite observations. *Journal of Hydrometeorology*, *9*(1), 22–47. https://doi.org/10.1175/2007JHM855.1

Neiman, P. J., Schick, L. J., Ralph, F. M., Hughes, M., & Wick, G. A. (2011). Flooding in Western Washington: The connection to atmospheric rivers*. *Journal of Hydrometeorology*, *12*(6), 1337–1358.

Niu, G.-Y., Yang, Z.-L., Mitchell, K. E., Chen, F., Ek, M. B., Barlage, M., et al. (2011). The community Noah land surface model with multiparameterization options (Noah-MP): 1. Model description and evaluation with local-scale measurements. *Journal of Geophysical Research*, *116*, D12109. https://doi.org/10.1029/2010JD015139

Oakley, N. S., Cannon, F., Munroe, R., Lancaster, J. T., Gomberg, D., & Ralph, F. M. (2018). Brief Communication: Meteorological and climatological conditions associated with the 9 January 2018 post-fire debris flows in Montecito and Carpinteria California, USA. *Natural Hazards and Earth System Sciences Discussions*, *2018*, 1–11. https://doi.org/10.5194/nhess-2018-179

Oakley, N. S., Lancaster, J. T., Kaplan, M. L., & Ralph, F. M. (2017). Synoptic conditions associated with cool season post-fire debris flows in the transverse ranges of Southern California. *Natural Hazard*, *88*(1), 327–354.

Pavelsky, T. M., Kapnick, S., & Hall, A. (2011). Accumulation and melt dynamics of snowpack from a multiresolution regional climate model in the central Sierra Nevada, California. *Journal of Geophysical Research*, *116*, D16115. https://doi.org/10.1029/2010JD015479

Pavelsky, T. M., Sobolowski, S., Kapnick, S. B., & Barnes, J. B. (2012). Changes in orographic precipitation patterns caused by a shift from snow to rain. *Geophysical Research Letters*, *39*, L18706. https://doi.org/10.1029/2012GL052741

Pierce, D. W., Cayan, D. R., & Thrasher, B. L. (2014). Statistical downscaling using Localized Constructed Analogs (LOCA). *Journal of Hydrometeorology*, *15*(6), 2558–2585.

Polade, S. D., Gershunov, A., Cayan, D. R., Dettinger, M. D., & Pierce, D. W. (2017). Precipitation in a warming world: Assessing projected hydro-climate changes in California and other mediterranean climate regions. *Scientific Reports*, *7*(1), 10783.

Polade, S. D., Pierce, D. W., Cayan, D. R., Gershunov, A., & Dettinger, M. D. (2014). The key role of dry days in changing regional climate and precipitation regimes. *Scientific Reports*, *4*, 4364.

Pontoppidan, M., Reuder, J., Mayer, S., & Kolstad, E. W. (1271). (2017), Downscaling an intense precipitation event in complex terrain: The importance of high grid resolution. *Tellus A: Dynamic Meteorology and Oceanography*, *69*(1), 561.

Ralph, F., Coleman, T., Neiman, P., Zamora, R., & Dettinger, M. (2013). Observed impacts of duration and seasonality of atmospheric-river landfalls on soil moisture and runoff in coastal northern California. *Journal of Hydrometeorology*, *14*(2), 443–459.

Ralph, F. M., Neiman, P. J., Kiladis, G. N., Weickmann, K., & Reynolds, D. W. (2010). *A multi-scale observational case study of a pacific atmospheric river exhibiting tropical-extratropical connections and a mesoscale frontal wave* (Vol. 139, pp. 1169–1189).

Ralph, F. M., Neiman, P. J., & Wick, G. A. (2004). Satellite and CALJET aircraft observations of atmospheric rivers over the eastern North Pacific Ocean during the winter of 1997/98. *Monthly Weather Review*, *132*(7), 1721–1745. https://doi.org/10.1175/1520-0493(2004)132<1721:SACAOO>2.0.CO;2

Ralph, F. M., Neiman, P. J., Wick, G. A., Gutman, S. I., Dettinger, M. D., Cayan, D. R., & White, A. B. (2006). Flooding on California's Russian River: Role of atmospheric rivers. *Geophysical Research Letters*, *33*, L13801. https://doi.org/10.1029/2006GL026689

Ralph, F. M., Rutz, J. J., Cordeira, J. M., Dettinger, M., Anderson, M., Reynolds, D., et al. (2019). A scale to characterize the strength and impacts of atmospheric rivers. *Bulletin of the American Meteorological Society*, *100*(2), 269–289.

Ralph, F., Wick, G., Neiman, P., Moore, B., Spackman, J., Hughes, M., et al. (2012). Atmospheric rivers in reanalysis products: A six-event comparison with aircraft observations of water vapor transport. In Extended Abstracts WCRP Reanalysis Conf. Silver Spring MD.

Rasmussen, R., Liu, C., Ikeda, K., Gochis, D., Yates, D., Chen, F., et al. (2011). High-resolution coupled climate runoff simulations of seasonal snowfall over Colorado: A process study of current and warmer climate. *Journal Climate*, *24*(12), 3015–3048.

Rienecker, M. M., Suarez, M. J., Gelaro, R., Todling, R., Bacmeister, J., Liu, E., et al. (2011). MERRA: NASA'S modern-era retrospective analysis for research and applications. *Journal of Climate*, *24*(14), 3624–3648.

Rummukainen, M. (2010). State-of-the-art with Regional Climate Models. *Wiley Interdisciplinary Reviews: Climate Change*, *1*(1), 82–96.

Rutz, J. J., Steenburgh, W. J., & Ralph, F. M. (2014). Climatological characteristics of atmospheric rivers and their inland penetration over the western United States. *Monthly Weather Review*, *142*(2), 905–921.

Satoh, M., Tomita, H., Yashiro, H., Kajikawa, Y., Miyamoto, Y., Yamaura, T., et al. (2017). Outcomes and challenges of global high-resolution non-hydrostatic atmospheric simulations using the k computer. *Progress in Earth and Planetary Science*, *4*(1), 1–24.

Shields, C. A., & Kiehl, J. T. (2016). Simulating the pineapple express in the half degree community climate system model, CCSM4. *Geophysical Research Letters*, *43*, 7767–7773. https://doi.org/10.1002/2016GL069476

Shields, C. A., Rutz, J. J., Leung, L.-Y., Ralph, F. M., Wehner, M., Kawzenuk, B., et al. (2018). Atmospheric River Tracking Method Intercomparison Project (ARTMIP): Project goals and experimental design. *Geoscientific Model Development*, *11*(6), 2455–2474.

Skamarock, W. C., & Klemp, J. B. (2008). A time-split nonhydrostatic atmospheric model for weather research and forecasting applications. *Journal of Computational Physics*, *227*(7), 3465–3485.

Smith, R. B. (1979). The influence of mountains on the atmosphere. *Advances in Geophysics*, *21*, 87–230.

Sun, F., Hall, A., Schwartz, M., Walton, D. B., & Berg, N. (2016). Twenty-first-century snowfall and snowpack changes over the Southern California mountains. *Journal Climate*, *29*(1), 91–110.

Swain, D. L., Langenbrunner, B., Neelin, J. D., & Hall, A. (2018). Increasing precipitation volatility in twenty-first-century California. *Nature Climate Change*, *8*(5), 427.

Swain, D. L., Lebassi-Habtezion, B., & Diffenbaugh, N. S. (2015). Evaluation of nonhydrostatic simulations of northeast Pacific atmospheric rivers and comparison to in situ observations. *Monthly Weather Review*, *143*(9), 3556–3569.

Thompson, G., Field, P. R., Rasmussen, R. M., & Hall, W. D. (2008). Explicit forecasts of winter precipitation using an improved bulk microphysics scheme. Part II: Implementation of a new snow parameterization. *Monthly Weather Review*, *136*(12), 5095–5115.

von Storch, H., Langenberg, H., & Feser, F. (2000). A spectral nudging technique for dynamical downscaling purposes. *Monthly Weather Review*, *128*(10), 3664–3673.

Walton, D., & Hall, A. (2018). An assessment of high-resolution gridded temperature datasets over California. *Journal Climate*, *31*(10), 3789–3810.

Walton, D. B., Hall, A., Berg, N., Schwartz, M., & Sun, F. (2017). Incorporating snow albedo feedback into downscaled temperature and snow cover projections for California's Sierra Nevada. *Journal Climate*, *30*(4), 1417–1438.

Warner, M. D., Mass, C. F., & Salathé, JrE. P. (2015). Changes in winter atmospheric rivers along the North American west coast in CMIP5 climate models. *Journal of Hydrometeorology*, *16*(1), 118–128.

Wrzesien, M. L., Durand, M. T., Pavelsky, T. M., Howat, I. M., Margulis, S. A., & Huning, L. S. (2017). Comparison of methods to estimate snow water equivalent at the mountain range scale: A case study of the California Sierra Nevada. *Journal of Hydrometeorology*, *18*(4), 1101–1119.

Zhu, Y., & Newell, R. E. (1998). A proposed algorithm for moisture fluxes from atmospheric rivers. *Monthly Weather Review*, *126*(3), 725–735.